

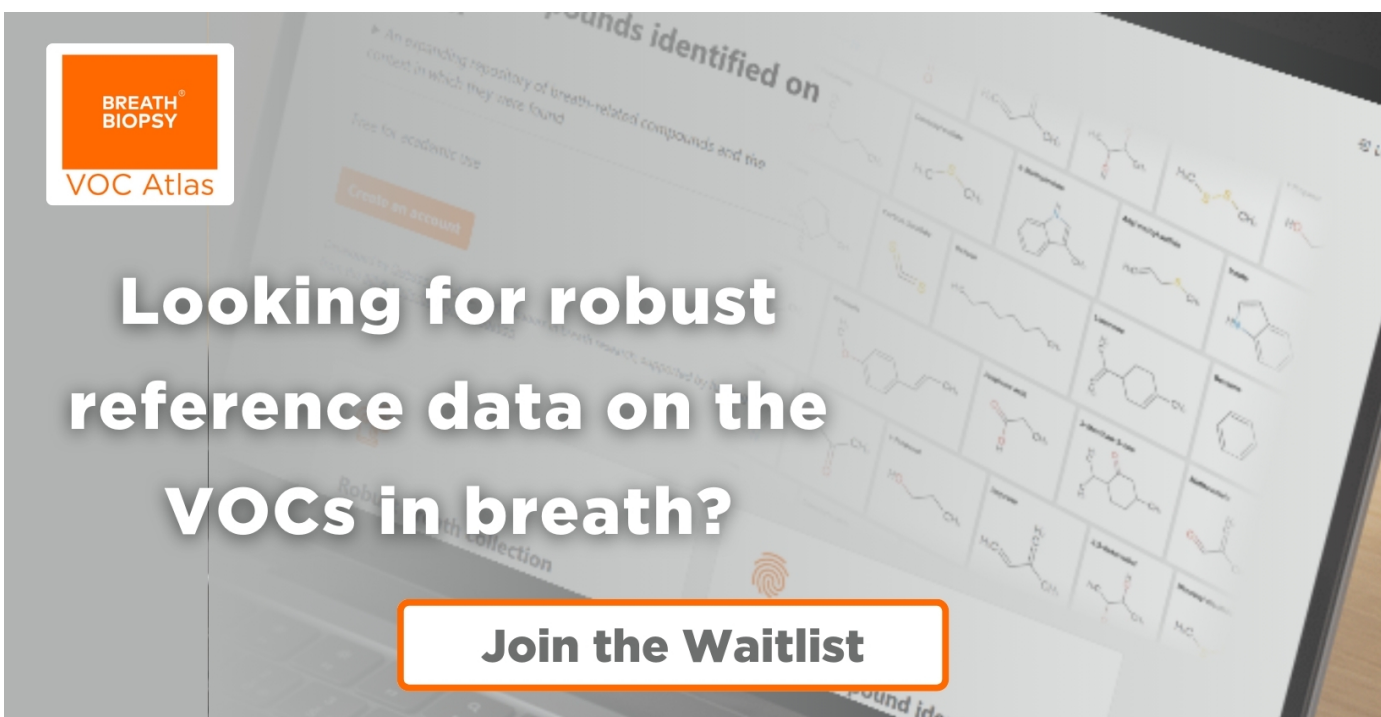
PAPER • OPEN ACCESS

Glycerol-blended chitosan membranes with directional micro-grooves and reduced stiffness improve Schwann cell wound healing

To cite this article: L Scaccini *et al* 2024 *Biomed. Mater.* **19** 065005View the [article online](#) for updates and enhancements.

You may also like

- [Methods to improve antibacterial properties of PEEK: A review](#)
Idil Uysal, Ayen Tezcaner and Zafer Evis
- [Advancements in stimulation therapies for peripheral nerve regeneration](#)
Rosalie Bordett, Khadija B Danazumi, Suranji Wijekoon *et al.*
- [Advances in electroactive bioscaffolds for repairing spinal cord injury](#)
Zeqi Liu, Jiahui Lai, Dexin Kong *et al.*



BREATH BIOPSY
VOC Atlas

An expanding repository of breath-related compounds and the context in which they are found

Free for academic use

Create an account

Looking for robust reference data on the VOCs in breath?

Join the Waitlist

ounds identified on

Robust breath collection

ound iden

The advertisement features a background image of a tablet displaying a grid of chemical structures. The text is overlaid on this image, with a prominent call to action 'Join the Waitlist' in a white box with an orange border.

170+
Compounds

100+
Diseases

500+
Literature Associations

Biomedical Materials



PAPER

OPEN ACCESS

RECEIVED
29 January 2024

REVISED
6 August 2024

ACCEPTED FOR PUBLICATION
29 August 2024

PUBLISHED
10 September 2024

Original content from this work may be used under the terms of the [Creative Commons Attribution 4.0 licence](https://creativecommons.org/licenses/by/4.0/).

Any further distribution of this work must maintain attribution to the author(s) and the title of the work, journal citation and DOI.



Glycerol-blended chitosan membranes with directional micro-grooves and reduced stiffness improve Schwann cell wound healing

L Scaccini¹ , A Battisti², D Convertino³, D Puppi⁴, M Gagliardi², M Cecchini² and I Tonazzini^{2,*}

¹ Laboratorio NEST, Scuola Normale Superiore, Piazza San Silvestro 12, 56127 Pisa, Italy

² INEST, Istituto Nanoscienze - Consiglio Nazionale delle Ricerche (CNR), Piazza San Silvestro 12, 56127 Pisa, Italy

³ Center for Nanotechnology Innovation @NEST, Istituto Italiano di Tecnologia, Piazza San Silvestro 12, 56127 Pisa, Italy

⁴ BIOLab Research Group, Department of Chemistry and Industrial Chemistry, University of Pisa, Udr INSTM—Pisa, Via G. Moruzzi 13, 56124 Pisa, Italy

* Author to whom any correspondence should be addressed.

E-mail: ilaria.tonazzini@cnr.it

Keywords: chitosan, scaffolds, nerve regeneration, Schwann cells, stiffness

Supplementary material for this article is available [online](#)

Abstract

Regenerative medicine is continuously looking for new natural, biocompatible and possibly biodegradable materials, but also mechanically compliant. Chitosan is emerging as a promising FDA-approved biopolymer for tissue engineering, however, its exploitation in regenerative devices is limited by its brittleness and can be further improved, for example by blending it with other materials or by tuning its superficial microstructure. Here, we developed membranes made of chitosan (Chi) and glycerol, by solvent casting, and micro-patterned them with directional geometries having different levels of axial symmetry. These membranes were characterized by light microscopies, atomic force microscopy (AFM), by thermal, mechanical and degradation assays, and also tested *in vitro* as scaffolds with Schwann cells (SCs). The glycerol-blended Chi membranes are optimized in terms of mechanical properties, and present a physiological-grade Young's modulus (≈ 0.7 MPa). The directional topographies are effective in directing cell polarization and migration and in particular are highly performant substrates for collective cell migration. Here, we demonstrate that a combination of a soft compliant biomaterial and a topographical micropatterning can improve the integration of these scaffolds with SCs, a fundamental step in the peripheral nerve regeneration process.

1. Introduction

Peripheral nerve injuries (PNIs) are a common condition around the world, with an incidence going from 13 to 23 cases per 100 000 persons every year [1]. Differently from the central nervous system, the peripheral nervous system presents a natural regenerative capability [2]. In small damages, the peripheral glial cells, called Schwann cells (SCs), undergo a phenotype switch, forming structures, called Bungner Bands, that provide a physical support to the regrowth of the nerve axon [3]. However, due to the tissue loss, in most cases and without a proper intervention, PNIs can lead to neuroma and scar tissue formation, with a subsequent loss of

nerve functionality [4]. Surgically, direct end-to-end suturing can be used only for small defects (< 5 mm), while for larger gaps the risk of worsening the damage is high, due to the strong tension that must be applied to the two stumps of the broken nerve [5]. Autologous and heterologous cell transplants are not diffuse for the low availability of SCs and because of safety and ethical concerns in the use of multipotent and pluripotent stem cells in clinics [6]. The gold standard for PNIs reparation in clinics remain the autologous nerve graft. Nonetheless, a shortage in donors, combined with the need for a second surgery to harvest the graft tissue, put limitations on this technique [7].

Neural scaffolds, such as nerve guidance conduits (NGCs), can be crucial in effectively accelerating

the regeneration process in PNIs, and in providing a structural support to the axon regrowth [8]. In recent years, a variety of different materials have been used to produce NGCs and some have already been approved for a clinical use, even if without conclusive results. A renewed interest in the development of nerve prostheses/interfaces was driven by the ability to manipulate novel biomaterials, controlling their surface topography, stiffness, or adaptable properties. To improve basic hollow conduits, different types of functionalization or engineering (e.g. material, porosity, protein coating, fillers, geometry) are under investigation [9]. It is now well known that neural cells can perceive nano and micro-topographical stimuli around them, both *in vivo* and *in vitro*. Neuronal and glial cells cultured on nano/micro-structured substrates actively tune their morphology, proliferation and migration [10]. Gratings patterns (GRs), anisotropic (directional) patterns of alternating lines of ridges and grooves, demonstrated their ability to polarize neuronal cells and SCs, and to direct their displacement [11–14]. In particular, we previously demonstrated that small-period GRs are particularly effective in driving collective SC migration and wound healing by contact guidance mechanism (i.e. features with a shorter period than the cell body diameter: line width < cell soma, $\approx 2\text{--}4\ \mu\text{m}$) [15]. Furthermore, it recently emerged that also the symmetry of the substrate's features can play a role in terms of cell responses. Interestingly, osteoblasts showed to modulate their shaping and migration speed in response to substrates with different levels of rotational symmetry [16]. Moreover, in a previous work, we demonstrated that SCs were guided by the underlying directional micro-topographies, but they also behaved according to the patterns' asymmetry [14]. Increasing the rotational asymmetry of the microtopography (using scalene (SCA) triangles pattern) leads to an improvement in the SCs migration ability, in comparison to GRs or isosceles triangles pattern (features with a lower rotational asymmetry). The most asymmetric directional pattern, with zig-zag SCA, polarized and aligned the RT4-SCs less strictly, leaving a higher degree of freedom for the nuclear/cell body orientation, but promoted a farther displacement of the cells with an increased persistence on one direction of migration, by inducing the establishment of asymmetric cell fronts with different actin fibers' organizations [14].

The need for new biocompatible materials in regenerative medicine is also driving research towards the study of natural biopolymers. One of these, chitosan (Chi), is gaining increasing interest for its availability and low costs. Chitosan is a deacetylation product of chitin, a major component of shrimps and other crustaceans' shells. Chitosan is completely biocompatible, non-immunogenic, biodegradable, and has been approved by the Food

and Drug Administration for its use in medical devices [17]. However, the use of Chi instead of other petroleum-based polymers has been limited by its physical characteristics: in fact, Chi films tend to be rigid and brittle. For this reason, plasticizers can be used to enhance the mechanical properties of Chi [18]. In this sense, polyols and glycerol, in particular, have been extensively tested [19, 20] and Chi films plasticized with glycerol resulted softer and more manageable [21]. The mechanism at the base of this ability consists in the capacity of the glycerol to interact with Chi chains, thus decreasing the number of interactions between them [20]. Several studies, using different concentrations of glycerol, demonstrated that the mechanical properties of Chi films (including stiffness) can be modulated by varying the concentration of the glycerol used [22]: in particular, higher amounts of glycerol lead to lower stiffness values. Glycerol-plasticized Chi films also have improved properties such as antibacterial activity, biocompatibility, water vapor permeability, and tensile strength [23, 24]. Basic plain Chi nerve conduits have been approved for clinical use in Europe: they can ameliorate peripheral nerve regeneration [25–27], however, their regeneration potential is still debated [28].

Mechanical features play pivotal roles in determining cell fate, too. The external stiffness is a key regulator of nervous tissue development/regeneration [29, 30] by triggering neurite outgrowth [31], SC behavior [32] or the gating of mechanosensitive Piezo receptors [33]. Therefore, it is important to take it into account and to develop mechanically compliant scaffolds for regenerative medicine applications. In this framework, nerves are soft tissues, with a Young's modulus value of about 0.5 MPa [34].

In this work, we developed, characterized and tested glycerol-blended chitosan (**Gly-Chi**) micro-structured membranes, aiming to improve the mechanical compliance between scaffolds and the peripheral nerve tissue but maintaining the topographical structures. **Gly-Chi** membranes with directional micro-topographies, presenting different levels of symmetry [GR and SCA] were produced by solvent casting and then tested *in vitro* with a glial SC line. We investigated nuclear, cell cytoskeleton and cell junctions' organization, Yes-associated protein (YAP) activation and glial markers expression, migration and wound-healing response, with the aim to develop improved scaffolds for nerve regeneration applications.

2. Results

2.1. Production and morphological characterization of Gly-Chi micro-patterned membranes

Gly-Chi membranes were microfabricated and patterned with anisotropic topographies of varying axial

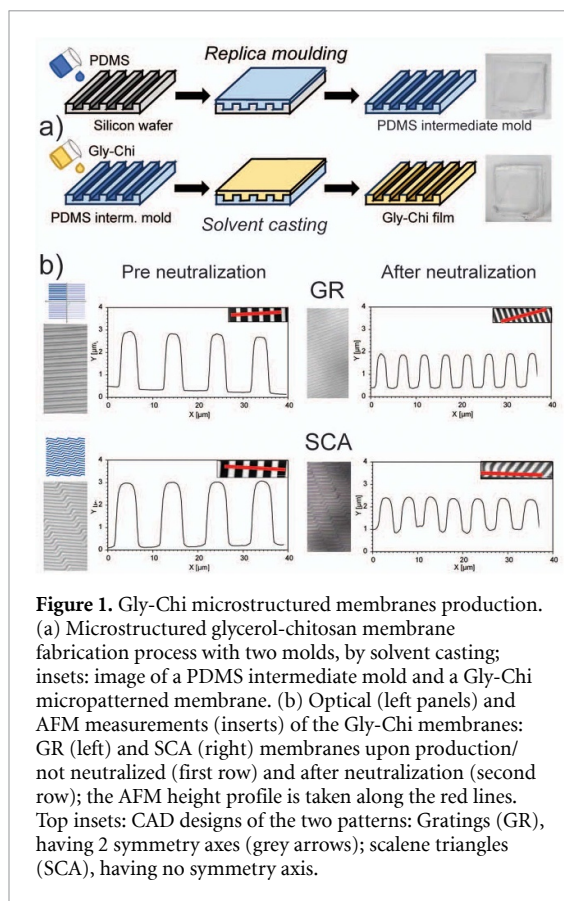


Figure 1. Gly-Chi microstructured membranes production. (a) Microstructured glycerol-chitosan membrane fabrication process with two molds, by solvent casting; insets: image of a PDMS intermediate mold and a Gly-Chi micropatterned membrane. (b) Optical (left panels) and AFM measurements (inserts) of the Gly-Chi membranes: GR (left) and SCA (right) membranes upon production/not neutralized (first row) and after neutralization (second row); the AFM height profile is taken along the red lines. Top insets: CAD designs of the two patterns: Gratings (GR), having 2 symmetry axes (grey arrows); scalene triangles (SCA), having no symmetry axis.

symmetry levels by solvent casting on polydimethylsiloxane (PDMS) intermediate molds (figure 1(a)). Patterns were transferred from silicon molds onto PDMS intermediate molds, following the procedure detailed in our previous work [14]. These molds were then utilized to structure a glycerol (10%)-Chi solution through solvent casting.

A 2% w/v Chi solution containing 10% v/v glycerol was poured onto the PDMS intermediate molds, and the solvent was allowed to evaporate under a chemical hood at room temperature (RT) for 72 h. Subsequently, Gly-Chi films were peeled off from PDMS. These membranes were soft, rubbery, and transparent, and the topographical features were well preserved on the Gly-Chi films (figure 1(a)-right). Two directional topographies were developed: GR, having two symmetry axes, and zigzag pattern with SCA, having no symmetry axis (figure 1(b)-insets). Isotropic flat membranes (FLAT) were also developed as control substrates. The PDMS molds used for solvent casting presented a period (i.e. the width of a ridge and a groove) of 10 μm , with 6 μm ridges and 4 μm grooves, and a depth of 2.5 μm .

The topographies created on Gly-Chi membranes were characterized using atomic force microscopy (AFM) (figure 1(b)). AFM measurements confirmed that the patterns had been successfully imprinted on Gly-Chi membranes during production (before neutralization) with the expected period of 10 μm

(comprising 4 μm ridges and 6 μm grooves). The heights of the features were as follows: $2.51 \pm 0.03 \mu\text{m}$ for GR and $2.86 \pm 0.03 \mu\text{m}$ for SCA (mean \pm SD) (table 1). We investigated the effects of the neutralization step (in 0.5% w/v NaOH for 30 min; necessary to prevent the solubilization of Gly-Chi films in water). After neutralization and subsequent drying, Gly-Chi dry membranes exhibited an approximate 50% reduction in pattern features (figure 1(b)-bottom row): the size reduction was $40 \pm 2\%$ for ridges, $53 \pm 3\%$ for grooves, and $53 \pm 2\%$ for depth, in both GR and SCA (table 1).

We then checked the effects of the exposure to liquids (i.e. water, PBS, cell culture medium) on our micro-structured membranes by optical imaging (figures 2(a) and (b)). Once in liquid, Gly-Chi films swelled immediately and the topographical features increased again in size, resulting in a pattern period of $7.6 \pm 0.3 \mu\text{m}$ for GR and $7.9 \pm 0.1 \mu\text{m}$ for SCA after 5 min in liquid. The patterns' size remained unaltered after longer exposure to liquid (after 24 h: $7.7 \pm 0.4 \mu\text{m}$ for GR and $7.8 \pm 0.3 \mu\text{m}$ for SCA, figure 2(a)). Importantly, Gly-Chi membranes soaked in liquid maintain their patterns stable and unchanged for long time, from days to several months (figures 2(a) and (b)-left column), independently from the liquid (water, PBS, culture media). In conclusion, the period size of Gly-Chi wet membranes was reduced of $24 \pm 3\%$ for GR and $22 \pm 3\%$ for SCA, compared to the original 10 μm period size.

Overall, we can develop stable and reproducible micro-grooved **Gly-Chi** membranes. Importantly, the addition of 10% glycerol allows retaining the pattern micro-topographical features and having more handleable films. After chemical neutralization, the patterns' dimensions are reduced on Gly-Chi membranes compared to the printing molds: the dimensionality reduction is $\approx 50\%$ for films in their dry state while it is only $\sim 23\%$ for wet films once in liquids.

2.2. Degradation, thermal and mechanical characterization of Gly-Chi micro-patterned membranes

The degradation profile of the Gly-Chi membranes was measured over the course of three months, in 10 and 100 mg l^{-1} solutions of lysozyme in PBS; a PBS solution was used as a control. To assess the pattern stability over time, Gly-Chi membranes were imaged in bright field over long time (figure 2(b)). The superficial patterns were still present on the membranes after 3 months. To measure the material degradation over time, membranes were weighed after the neutralization process ($t = 0$) and then weighed at selected time-points (3, 7, 14, 21 d and 1, 2 and 3 months). The change in weight over time is reported in figure 2(c). For all conditions, the weight loss increased over time, however in presence of the lysozyme solution, Gly-Chi membranes degradation was significantly

Table 1. AFM measurements quantification of micropattern features (mean \pm SD) for GR and SCA Gly-Chi membranes before neutralization and after neutralization; period = ridge width + groove width.

	Ridge width (μm)	Groove width (μm)	Period (μm)	Depth (μm)
GR (before neutralization)	3.52 ± 0.09	6.17 ± 0.27	9.7 ± 0.3	2.51 ± 0.03
GR- neutralized (dry)	2.08 ± 0.12	2.67 ± 0.12	4.8 ± 0.2	1.22 ± 0.02
SCA (before neutralization)	4.50 ± 0.05	5.59 ± 0.16	10.1 ± 0.2	2.86 ± 0.03
SCA- neutralized (dry)	2.71 ± 0.13	2.80 ± 0.16	5.5 ± 0.3	1.30 ± 0.10

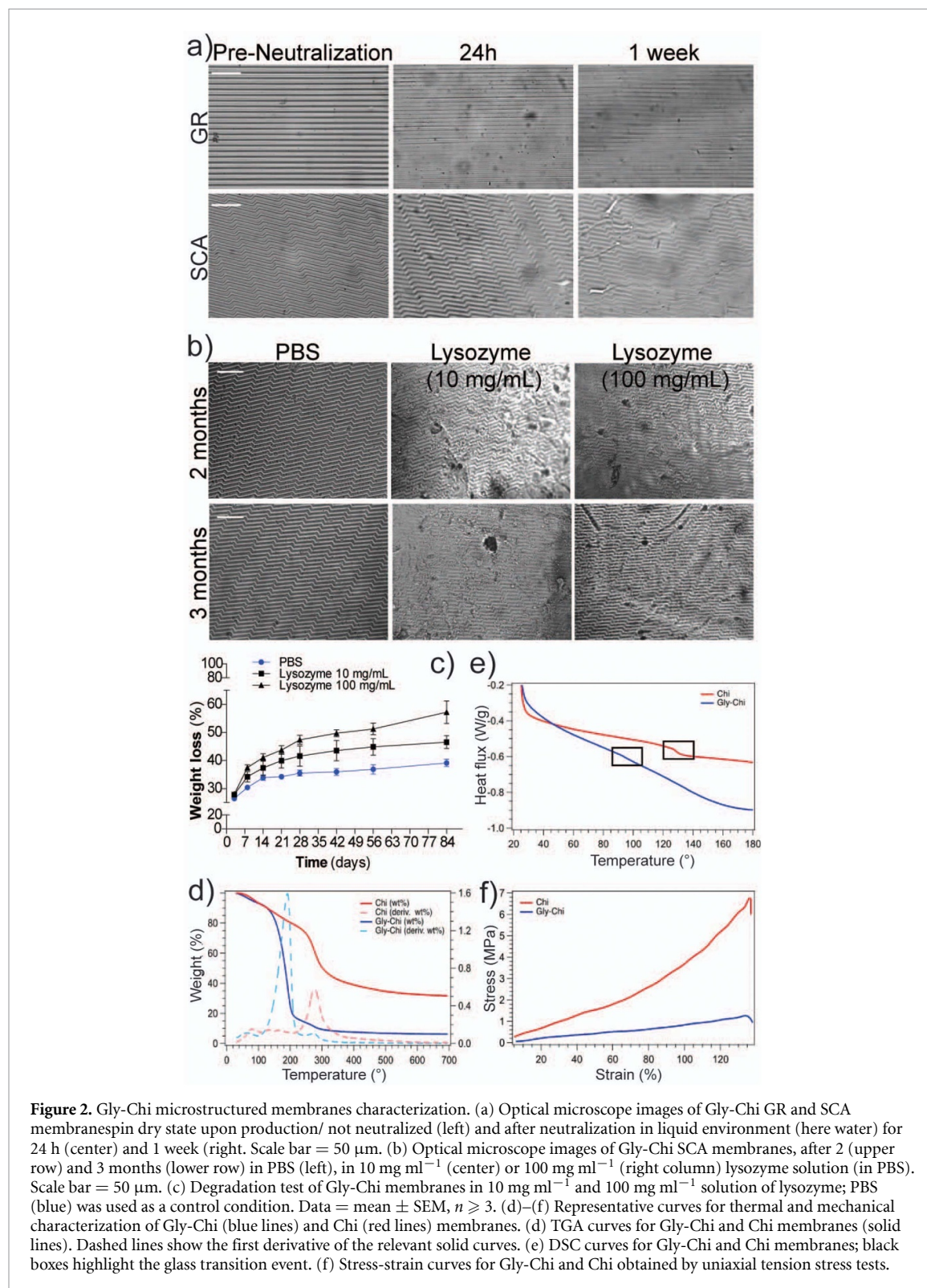


Table 2. TGA, DSC and uniaxial tension stress test average results for Gly-Chi and Chi (as in [14]) membranes; ¹ peak values in the first derivative of the thermogram curve.

Sample	Decomposition temperature (°C) ¹	T_g (°C)	Young's modulus (MPa)	Stress at break (MPa)	Strain at break (%)
Gly-Chi	192.3 ± 0.7	100 ± 10	0.7 ± 0.1	1.0 ± 0.4	131 ± 40
Chi	275.7 ± 1.4	115 ± 13	5 ± 1	5 ± 1	130 ± 11

enhanced ($P < 0.01/0.001$, PBS vs. 10 mg l⁻¹ lysozyme and vs. 100 mg l⁻¹ lysozyme, Bonferroni test). Overall, our Gly-Chi membranes maintain microtopography instructions over time, also in the presence of scaffold degradation.

The expected plasticizing effects of glycerol on the Chi films were evaluated by thermogravimetric analysis (TGA), differential scanning calorimetry (DSC), and uniaxial tension stress tests on Gly-Chi membranes in comparison to those of pure Chi (data are summarized in table 2). The TGA thermograms of pure Chi and of the Gly-Chi membranes are shown in figure 2(d). As expected, the TGA curve of Chi and Gly-Chi films showed two stages of weight loss. Overall, Gly-Chi films show a reduced thermal stability; however, decomposition occurs at temperatures well above the envisioned working temperature of the final scaffold. DSC analysis (figure 2(e)) revealed an average glass transition temperature (T_g) of about 115 °C for the pure Chi membranes. The addition of glycerol caused a drop of the average T_g to about 100 °C. This is in good agreement with the plasticizing effect exerted by glycerol, whose presence can interfere with the packing of the Chi chains [21]. Figure 2(f) shows a typical stress-strain curve for a Gly-Chi membrane, in comparison with a pure hydrated Chi membrane. Data (table 2) show that, even if Gly-Chi blended membranes have a similar average relative strain at break if compared to Chi ones, Gly-Chi membranes have a significantly lower Young's modulus (0.7 ± 0.1 MPa).

2.3. Effect of Gly-Chi microstructured substrates on SC morphology, polarization, YAP activation and glial markers expression

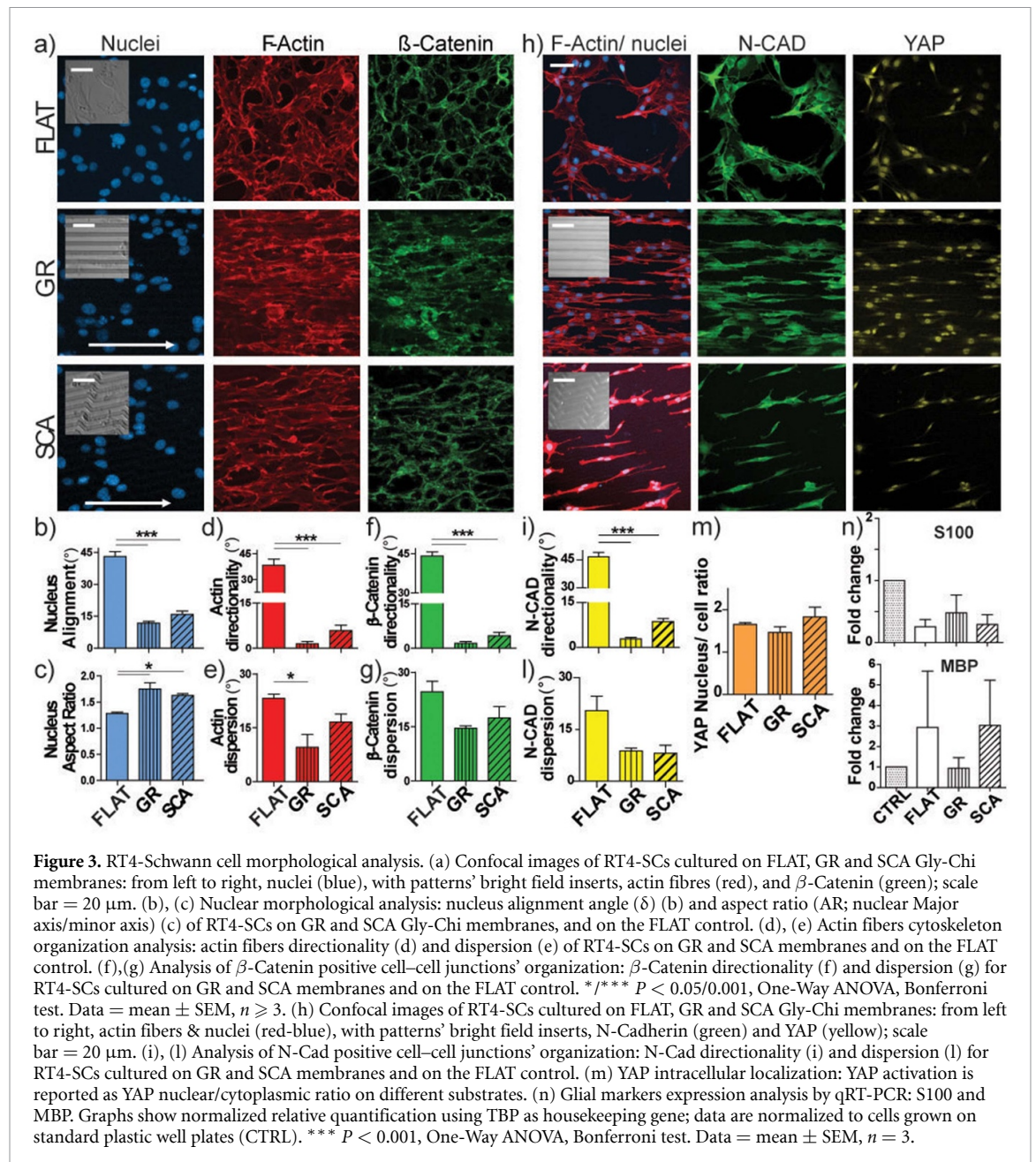
We tested our Gly-Chi membranes *in vitro* with RT4-SCs, a SC line (RT4-D6P2T) stably expressing the green-fluorescent-protein (GFP), to assess their ability to direct and improve SC polarization and migration.

RT4-SCs adhered and grew well on Gly-Chi membranes, reaching cell confluence on Gly-Chi membranes in standard times. We analyzed the morphology of RT4-SCs cultured on our films by staining cells for nuclei, actin fibers, and cell-cell junctions (figures 3(a) and (h)). We quantified two nuclear shape-defining parameters: alignment angle°; (in respect to the pattern orientation; figure 3(b)) and aspect ratio (ratio of its major axis to its minor

axis; figure 3(c)). Nuclei aligned along GR and SCA patterns, at a similar extent (FLAT 43 ± 2°, GR 12 ± 1°, SCA 16 ± 2°; $P < 0.001$ vs. FLAT, Bonferroni test; figure 3(b)), and were more elongated accordingly ($P < 0.05$ GR and SCA vs. FLAT, Bonferroni test; figure 3 (c)), while on FLAT nuclei were rounded shaped. We then analyzed the organization of the cytoskeleton in RT4-SC layers on our Gly-Chi membranes. Actin fibers orientation was quantified by Fast Fourier Transform (FFT) analysis of the fluorescent images, which returns the actin fibers' signal dispersion (i.e. indicator for the angular spread of the actin fluorescence signal) and directionality (an indicator for the overall degree of orientation of the cytoskeleton fibers, here normalized versus the underlying pattern direction) (figures 3(d) and (e)). As expected, both the patterns were highly efficient in orientating RT4-SC actin fibers ($P < 0.001$ vs. FLAT, Bonferroni test), while on the FLAT cells were randomly oriented (average angle ≈ 45°; figure 3(d)). GR decreased significantly the dispersion of actin signal ($P < 0.05$, FLAT vs. GR, Bonferroni test), by highly polarizing the fibers along the GR pattern, while SCA was not efficient in this framework and presented intermediate values (figure 3(e)).

We then investigated the effects of topography on cell-cell interactions, by looking at the adherent junctions via β -Catenin and N-Cadherin markers' expression (figures 3(a) and (h)). Both β -Catenin and N-Cadherin expression pattern was analyzed using the same method presented for actin. The localization of β -Catenin developed oriented and aligned to the patterns, while it appeared randomly organized on FLAT. We found that both GR and SCA guided β -Catenin orientation ($P < 0.01$ vs. FLAT, Bonferroni test; figure 3(f)), however they had almost no impact on its dispersion (figure 3(g)), leaving a high degree of freedom to β -Catenin organization. We observed an analogous behavior on the signal distribution of the N-Cadherin (figures 3(i)-(l)), confirming the orientation of cell-cell junctions on both GR and SCA, at a similar extent.

Overall, Gly-Chi membranes are well suitable substrates for SCs. These data demonstrate that both GR and SCA Gly-Chi membranes are effective in inducing SC polarization and alignment along the patterns, at nuclear, cytoskeleton, and cell-cell junctions' levels. The more asymmetric pattern, SCA, just leaves a higher degree of freedom to cell cytoskeleton,



showing a higher dispersion of the actin fibers signal. Altogether, these data demonstrate that soft Gly-Chi directional patterns guide RT4-SCs, but RT4-SCs are not influenced by their asymmetry level.

We finally investigated the involvement of YAP/TAZ signaling in cell contact guidance on our soft Gly-Chi topographies. Once activated by mechanical signals, YAP concentrates into the nucleus, thus we performed immunostaining for YAP to investigate its intracellular localization in response to the different Gly-Chi topographies (figures 3(h) and (m)). The nuclear/cytoplasm YAP ratio was similar on the different substrates (figure 3(m)).

Finally, the mRNA expression level of glial markers, S100 and myelin basic protein (MBP), and of brain-derived neurotrophic factor (BDNF) was examined by quantitative real-time PCR (qRT-PCR)

in RT4-SCs cultured on our FLAT, GR and SCA Gly-Chi membranes. S100 resulted well and equally expressed in RT4-SCs cultured on the different Gly-Chi patterns and on the standard plastic plate (figure 3(n)). The expression of MBP was also stable but really low in our RT4-SCs (figure 3(n)). Similarly, the mRNA expression level of BDNF was also really low in our samples (figure S1(a)). We also performed additional analysis ($n = 2$) using HPRT1 as housekeeping gene, and we obtained the same results (figures S1(b)–(d)). In conclusion, data confirm that RT4-SCs are not influenced by the different topographies on softer Gly-Chi membranes.

Our previous work [14] indicated the presence of an asymmetric protrusion organization and a consequent asymmetric cell contractility status in RT4-SCs growing on SCA topographies made of full Chi.

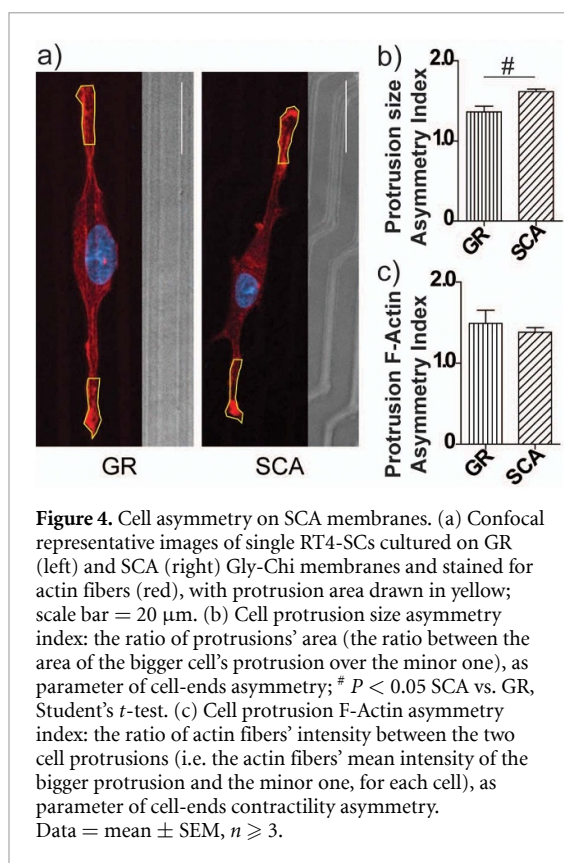


Figure 4. Cell asymmetry on SCA membranes. (a) Confocal representative images of single RT4-SCs cultured on GR (left) and SCA (right) Gly-Chi membranes and stained for actin fibers (red), with protrusion area drawn in yellow; scale bar = 20 μm . (b) Cell protrusion size asymmetry index: the ratio of protrusions' area (the ratio between the area of the bigger cell's protrusion over the minor one), as parameter of cell-ends asymmetry; # $P < 0.05$ SCA vs. GR, Student's t -test. (c) Cell protrusion F-Actin asymmetry index: the ratio of actin fibers' intensity between the two cell protrusions (i.e. the actin fibers' mean intensity of the bigger protrusion and the minor one, for each cell), as parameter of cell-ends contractility asymmetry. Data = mean \pm SEM, $n \geq 3$.

We analyzed the terminal protrusions of RT4-SCs on Gly-Chi films, by measuring the ratio between the two cell protrusions' areas (figure 4(a)). We quantified this cell-ends size asymmetry index by calculating the ratio between the bigger side and the minor one of each cell (i.e. therefore the ratio is always >1 , even if the two sides have similar cell-end areas). RT4-SCs were mainly bipolarized on Gly-Chi patterns, as expected. The two main cytoplasmatic protrusions extend almost equally in both side of the cells on GR, resulting in a similar area of both edges. As expected, on SCA instead one cell end was consistently larger than the other, and here the substrate asymmetry led to an increase in the area asymmetry ratio between the two protrusion edges in cells ($P < 0.05$ SCA vs. GR, Student's t -test; figure 4(b)). We then analyzed the intensity of actin fibers, by quantifying the ratio of the actin signal intensity between the two cell-ends for each cell, such as an index of actin contractility asymmetry. We found no difference both in GR and SCA (figure 4(c)).

Overall, SCA induces the establishment of asymmetric cell fronts in RT4-SCs, caused by the local topographical differences encountered by each cytoplasmatic protrusion during cell motion, but not an asymmetric actin organization.

2.4. SC migration along Gly-Chi microstructured substrates

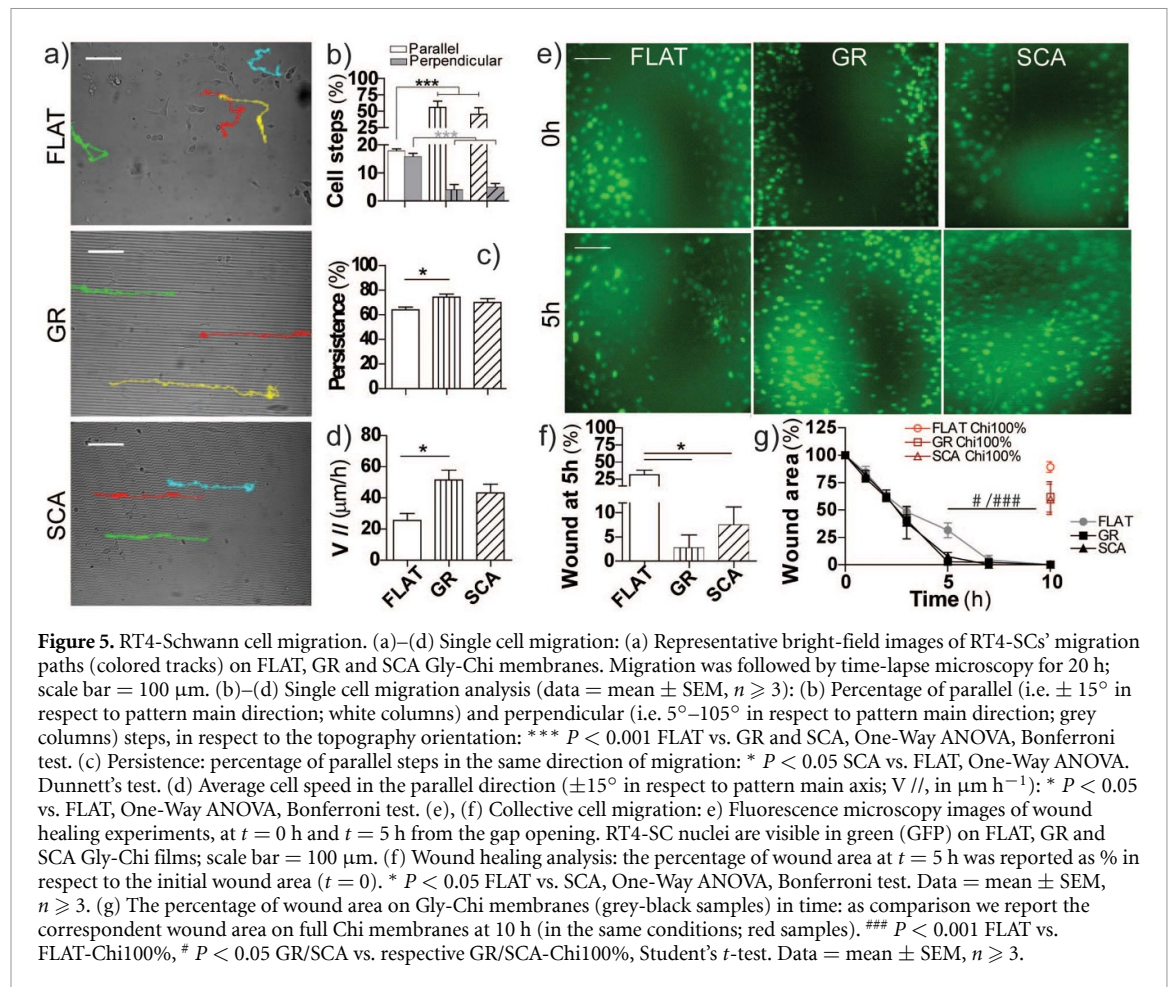
The migration of single RT4-SCs on Gly-Chi membranes was tested (figure 5(a)). Cells migrated mostly

parallel to the main axes of the topographies, while maintained a random walk on flat membranes: the percentage of parallel ($\pm 15^\circ$) steps increased (figure 5(b)) from $18 \pm 1\%$ for FLAT (i.e. for random motion with an arbitrary reference direction, the aligned steps would theoretically be 20%) to $56 \pm 9\%$ for GR, and $45 \pm 10\%$ for SCA ($P < 0.001$ vs. FLAT, Bonferroni test). Accordingly, the migration along the perpendicular direction was significantly inhibited and the number of perpendicular steps decreased below 5% on both GR and SCA ($P < 0.001$ vs. FLAT; figure 5(b)).

Regarding the persistence of the cell motion along one direction of a migration path (i.e. in parallel to the pattern), RT4-SCs persisted for more time migrating on one specific direction on GR ($74.4 \pm 2.4\%$ steps; $P < 0.05$ GR vs. FLAT, Bonferroni test) but only at a minor extent on SCA ($70 \pm 3\%$ steps), and FLAT condition ($63.9 \pm 2.2\%$ steps) (figure 5(c)). RT4-SCs moved significantly faster along GR and SCA patterns ($V_{\parallel} = 51.4 \pm 6.4 \mu\text{m h}^{-1}$, and $43.3 \pm 5.5 \mu\text{m h}^{-1}$, respectively) compared to FLAT ($V = 25.4 \pm 4.5 \mu\text{m h}^{-1}$; $P < 0.05$ vs. FLAT, Bonferroni test) (figure 5(d)). Generally, GR ($269 \pm 28 \mu\text{m}$) and SCA ($196 \pm 74 \mu\text{m}$) Gly-Chi films had only a mild positive effect on the final cell displacement compared to FLAT ($77 \pm 46 \mu\text{m}$; $P < 0.05$ GR vs. FLAT, Bonferroni-selected test). Overall, both GR and SCA Gly-Chi membranes direct and speed up single RT4-SC migration along the patterns (in terms of parallel steps and speed). However, the migration at single cell level was not significantly improved, either tuned by the asymmetry in the pattern. Here, the best performing pattern is GR, that promotes cell directional displacement and higher persistence along one direction of migration.

We then performed wound healing experiments (figure 5(e)). The cell collective migration was observed via time-lapse microscopy up to wound closure, and the wound area was reported as the percentage of wound area present at $t = 5$ h compared to the initial ($t = 0$) wound area. The initial gap mean width was similar between different substrates ($291 \pm 24 \mu\text{m}$ for GR, $319 \pm 31 \mu\text{m}$ for SCA and $290 \pm 56 \mu\text{m}$ for FLAT). The microstructured Gly-Chi membranes induced a faster collective migration into the gap: after 5 h the wound area was already significantly reduced on both GR and SCA ($P < 0.05$ vs. FLAT, Bonferroni test, figure 5(f)), with no further effects of the pattern asymmetry. The number of cells on Gly-Chi substrates was quantified at $t = 24$ and 48 h, and the cell proliferation was similar on the different substrates (figure S2(a)).

The wound area closure in time (figure 5(g)) proceeded fast on Gly-Chi membranes. As a comparison, we report that the wound area on correspondent Chi 100%-membranes (seeded in the same conditions and with similar initial gaps, as in [14]; figure 5(g)) was still significantly bigger after 10 h in comparison



to the correspondent topography on Gly-Chi films after 5 h ($P < 0.001$ FLAT Gly-Chi vs. FLAT Chi; $P < 0.05$ GR Gly-Chi vs. GR Chi and SCA Gly-Chi vs. SCA Chi; Student's t -test).

Here, both GR and SCA Gly-Chi films significantly boost collective RT4-SC cell migration. Overall, glycerol blending is particularly effective in improving SC wound healing.

3. Discussion

In this work, we developed **Gly-Chi** soft membranes structured with reproducible directional and asymmetric micro-topographies, *via* a solvent-free and RT process. The Gly-Chi membranes present not only stable topographic features but also optimal mechanical compliance for SCs. Indeed, the blend's final Young's modulus of 0.7 MPa closely approaches the physiological stiffness of nerve tissues. Both Gly-Chi GR and SCA topographies are effective in inducing RT4-SCs nuclear and cytoskeletal alignment to the pattern, tuning their cell-cell junctions with a certain degree of freedom, and directing cell migration accordingly. The asymmetry in the directional pattern (i.e. SCA), however, does not influence RT4-SCs behavior, at the level of morphology, YAP activation

and glial markers expression, and, in particular, does not induce an asymmetric organization of actin fibers at the cell leading edges. Importantly, Gly-Chi soft membranes improve *per se* the cell collective migration performance of RT4-SCs.

Although Chi has demonstrated to be an interesting material for biomedical applications, for its biocompatibility, non-immunogenicity, and biodegradability, pure Chi membranes are rigid [35] and tend to break easily, thus being not ideal to be used as scaffolds for regenerative medicine. Here, glycerol was used as an effective plasticizer, as it is known that it helps the reduction of the natural stiffness of Chi. Since Chi is a semicrystalline polymer, this effect can be attributed to crystalline disorder induced by glycerol and by the water molecules that this hydrophilic additive attracts within the polymeric matrix [20]. Thanks to its low molecular weight and small size, glycerol can easily penetrate between the Chi chains. The three—OH groups allow glycerol forming stable hydrogen bonds with Chi while increasing the chains mobility, thus making the Gly-Chi matrix both more flexible and hydrophilic. We tested various concentrations of Gly, ranging from ≈ 5 to 20%. The decision to use a 10% v/v concentration depends on the fact that this is the higher concentration able to

not compromise our GR and SCA topographical features and their structural integrity. At Gly concentrations higher than 10%, we observed Gly-Chi membranes that lose their coherence, leading to the loss of the superficial microstructures after the treatment with the neutralizing solution. For Gly concentrations $\leq 10\%$, we did not observe any change in the consistency of the material and in the micro-structured features. Importantly, the stiffness of our 10% glycerol-Chi membranes is almost seven times smaller than the value of pure Chi [35], with a value approaching the physiological value of nerve tissues (≈ 0.5 MPa [34]). The thermal characterization proved that glycerol lowers the matrix T_g : the DSC curves showed a shift in T_g from about 115°C to 100°C , thus the matrix still is in its glassy state when used at RT or under physiological conditions. TGA experiments revealed that the presence of glycerol significantly alters the onset of the degradation temperature. For Chi samples, the first weight loss stage occurred in the range 50°C – 100°C and was mainly attributed to the evaporation of water molecules or residual acetic acid [36], with a weight loss of about 10%; then the primary degradation of Chi started at about 253°C , leading to complete degradation at 450°C , with a weight loss of about 40%, as expected [37]. On the other side, the thermogram of Gly-Chi membranes showed the same initial weight loss due to water and acetic acid evaporation, then the polymer decomposition stage occurred between 150°C and 310°C , with a weight loss of about 80%. This marked difference in terms of residual weight at 700°C can be related to different aspects, including the lower thermal stability of Gly in comparison to Chi, Gly hygroscopic nature, as well as a weakening of intermolecular hydrogen bonds between Chi chains as a consequence of Gly plasticizing effect. The small band around 290°C can be attributed to the evaporation of glycerol molecules. In Gly-Chi membranes, then, the decomposition temperature under inert atmosphere drops by more than 80°C ; however, this value falls well beyond the expected working temperature range of the final devices ($\approx 37^\circ\text{C}$), and operatively the presence of the plasticizer has no adverse effects on the properties of the matrix.

Our membranes were obtained through a solvent casting procedure, starting from silica molds and using intermediate PDMS molds. This double-step procedure presents the advantages already discussed in [35]. After the drying process of the Gly-Chi membranes, a deprotonation of the amine groups with a 0.5% NaOH solution is necessary (i.e. to avoid the solubilization in water solutions). This concentration and time treatment allows a non-aggressive process. The resulting dimensionality shrinkage ($\approx 25\%$) of Gly-Chi topographies can be attributed to a release

of water from the bulk structure. However, the smaller period size obtained (ridge+ groove period ≈ 7.5 – $8\ \mu\text{m}$ for films in liquid conditions, in respect to the original $10\ \mu\text{m}$ period) fits the size for a contact guidance mode (i.e. structures with a shorter period than the cell body diameter) of interaction between the substrates and SC cells, which was demonstrated to be particularly effective in wound healing performance according to our previous work [15].

We simulated the exposure of our membranes to physiological conditions, using lysozyme solutions at increasing concentrations, as it is known that lysozyme is overexpressed in the PNI environment [38]. Our microstructured Gly-Chi membranes are able to retain the superficial patterns stably over time, up to 3 months. This feature is requested for nerve regenerative applications, as the regeneration process needs months to be correctly carried out [39].

We tested our membranes *in vitro* with a SCs model. Here, both GR and SCA topographies improved a directional and farther displacement of RT4-SCs equally, and GR was almost the most efficient substrate in increasing cells' speed and persistence in one direction of migration. Overall, RT4-SCs were guided by both our directional Gly-Chi microtopographies but they did not respond to the patterns' different asymmetry, as we found instead on fully Chi membranes with the almost same topographies [14]. We demonstrated previously that SCA pattern (i.e. the directional topographies with the higher degree of asymmetry) in pure Chi substrates induces SC bipolarization and the establishment of asymmetric cell fronts with different actin fibers content at the cell's edges, and proposed that this mechanism improves in turn the RT4-SCs migration performance on SCA [14]. Here, SCA Gly-Chi films induced cell bipolarization, and the establishment of asymmetric edges (in size) but not an asymmetric actin fibers content between the two cell edges (figure 4(b)). These data suggest that the lack of a leading edge with a higher fibers' content in RT4-SCs on SCA Gly-Chi films is related to the loss of SCA primacy in inducing directional persistence in migration. The equal level of actin fibers between the cell tips can explain the loss of the asymmetry's influence of the pattern's asymmetry and the absence of enhanced single cell migration on SCA Gly-Chi substrates. Our data suggest that the low(er) stiffness of Gly-Chi membranes abolish the influence of the asymmetry of the directional pattern on RT4-SCs. In line with this, SCs are capable of durotaxis, and highly sensitive detectors of mechanical heterogeneity. Previous works which studied the influence of substrate stiffness on the behavior and functions of SCs showed that SCs: do not migrate differently on uniform substrates of different stiffness but respond

differently to stiffness gradients [32]; present an optimal elastic modulus value responsible for the best SC migration behavior (i.e. 7.45 kPa), more than a dependency between the stiffness and the SC responses [40].

If we compare the morphological parameters of RT4-SCs on Gly-Chi membranes versus the same cells on Chi membranes with same microtopographies (from [14]), we find that on Gly-Chi films: (i) nuclei present similar alignment angle but a lower nuclear elongation ($P = 0.05$ Gly-Chi GR vs. Chi GR, $P < 0.001$ Gly-Chi SCA vs. Chi SCA, Student's t -test; figure S2(b)); (ii) actin fibers are similarly organized for alignment and dispersion (figure S2(c)); (iii) the cell edges show a reduction of both area asymmetry ratio ($P < 0.01$ Gly-Chi GR vs. Chi GR, and Gly-Chi SCA vs. Chi SCA; Student's t -test; figure S2(d)) and actin fibers' asymmetry ratio ($P < 0.01$ GR vs. GR and SCA vs. SCA; Student's t -test; figure S2(e)). Comparing the migration of single RT4-SCs figures S2(f)–(h), on Gly-Chi membranes there is: (i) no difference in the cell guidance along the pattern main direction; (ii) almost no difference in the persistence of cells' motion, even if SCA show a decreasing trend in this value ($P = 0.06$ Gly-Chi SCA vs. Chi SCA, Student's t -test); (iii) a reduction in the cell speed, in particular on Flat and SCA ($P < 0.05$ Gly-Chi Flat vs. Chi Flat, and Gly-Chi SCA vs. Chi SCA, Student's t -test), while not on GR. Importantly, Gly-Chi films significantly boosted RT4-SCs collective migration compared to Chi films (figure 5(g)). Overall, a direct comparison indicates that on Gly-Chi membranes with lower stiffness the influence of the asymmetry of SCA pattern on RT4-SCs is almost abolished. However, altogether these experiments indicate that both GR and SCA Gly-Chi films are efficient in guiding SCs and improve their wound healing.

We can speculate that in this framework the role of actin cytoskeleton is relevant, in fact cell migration is mediated by actin contractility. It is generally accepted that stiff substrates facilitate faster and more directional cell polarization and faster migration [41], because cells can better generate the necessary traction forces, leading to the formation of larger focal adhesions and a more extensive cytoskeletal network. On the other end, on soft(er) substrates the actin cytoskeleton is highly dynamic, leading to a decrease of tension [42]. Comparing the morphological parameters of RT4-SCs on Gly-Chi membranes versus the same cells on pure Chi membranes with similar microtopographies (figure S2), cells showed reduced nuclear polarization, and reduced asymmetric organization of the edges, in line with the general rule. Moreover, on Gly-Chi substrates, RT4-SCs at single level migrated almost slower than on the stiffer pure Chi membranes (figure S2(h)), in line with this general expected cells' behavior [42]. When comparing

the collective cell migration data after 10 h on Gly-Chi versus Chi membranes, we find a substantial difference: their wound healing was importantly improved. The different migration responses at single and collective levels on Gly-Chi substrates call in cause the cell–cell interactions, as previously in our experience. We indeed showed that GR topographies in the regime of contact guidance mode (i.e. line width $<$ cell soma, $\approx 2\text{--}4\ \mu\text{m}$) were more effective in inducing wound healing, thus allowing higher N-Cadherin cell–cell contacts [15]. Here, again the cell–cell interactions likely play a role in the migration behavior. When cells grow in a monolayer, they form adherens junctions which are mediated by proteins like cadherins and catenins and link the actin cytoskeleton of adjacent cells. N-/E-Cadherin forms the core of the SCs adherens junctions and requires association with its cytoplasmic partner β -Catenin, which provides a link to the cytoskeleton [43] and interact with Hippo/YAP pathway [44]. As expected, here N-Cad-positive junctions resemble the β -Catenin signal. Both β -Catenin and N-Cadherin signals in RT4-SCs were well polarized by GR and SCA Gly-Chi, but maintained a high dispersion (i.e. almost similar to flat substrates), thus suggesting optimal cell–cell interactions and well distributed cell-to-cytoskeleton spots on RT4-SCs cell layers on our low-stiffness substrates. Gly-Chi microstructured substrates, more compliant with the physico-mechanical features of nervous tissues *in vivo*, highly contributes to the faster wound healing of RT4-SCs.

We also decided to look at the YAP activation in response to the different Gly-Chi topographies, because this protein (i.e. a transcriptional co-regulator that regulates gene transcription) is known for its association with the acto-myosin cytoskeleton and N-cadherin and β -catenin in the transduction of mechanical stimuli. Mechanical stimuli (e.g. N-cadherin mediated cell adhesion) activate Yap activity by its phosphorylation, which in turn relocates Yap to the nucleus [44]. Previously, we demonstrated that PC12 cells have an increased YAP nuclear localization (and hence YAP activation) if cultured on nano-grating topographies (line width 100–500 nm), with respect to those on Flat substrates [45]. However, here the different geometries of Gly-Chi membranes were not able to tune YAP nuclear translocation and overall, YAP does not seem relevant in RT4-SCs contact guidance response on Gly-Chi substrates.

RT4-SCc grown on Gly-Chi well expressed S100 mRNA, as expected for these cells [46]. The expression levels of MBP and BDNF (that can be produced by SCs, supporting their migration [47]) showed a high variability, which is probably dependent on the very low expression of these genes in our RT4-SCs: in fact, these results showed always Ct values > 35 . In conclusion, the levels of glial markers' expression

either the expression (production) of BDNF in RT4-SCs are not influenced by the Gly-Chi membranes or by their different geometries.

Overall, the possibility to produce **Gly-Chi** soft films with stable directional micro-topographies, both GR and SCA, can be useful for applications in peripheral nerve regeneration, as mechanically compliant and micro-structured materials could be of particular interest in creating a new generation of improved conduit scaffolds.

3.1. Conclusions

In this work, we show that soft microstructured **Gly-Chi** membranes can be produced through a simple, cheap and reproducible solvent casting procedure. Our membranes and their superficial micropatterns are stable over time for several months, also in simulated physiological conditions. The 10% glycerol blending reduces importantly the stiffness of the material while the superficial microstructures, even though presenting a slight reduction in their dimensions ($\approx 22\%$), are stable and allow an optimal SC compatibility and guidance *in vitro*. The two micro-topographies tested, GR and SCA, led to almost equal cell migration performance and importantly these softer GR and SCA Gly-Chi membranes improve significantly the collective migration performance of RT4-SCs compared to pure Chi membranes. Our soft membranes demonstrated optimal mechanical properties and *in vitro* results, compatible with their further use in biomedical applications. Here, we demonstrate that a combination of a soft compliant material and a topographical micropatterning can improve the integration of these scaffolds with SCs, a fundamental step in the peripheral nerve regeneration process.

4. Material and methods

4.1. Micro-patterned molds and polydimethylsiloxane intermediate molds development

The silicon molds were developed through photolithography technique, as previously described [14]. The following directional micro-patterns were developed: GR, with alternating lines of grooves and ridges; zigzag pattern with SCA. FLAT control patterns were also developed, as control condition. The GR and SCA patterns were designed with a period of 10 μm , 4 μm of ridges and 6 μm of grooves, and depth of 2.5 μm . Then PDMS intermediate mold replicas were realized with the silanized silicon molds, as previously described [14]. The PDMS intermediate replicas were used for the fabrication of blended Chi films, through a solvent casting technique.

4.2. Gly-Chi membrane fabrication

The Chi solution 2% w/v was prepared using Chi medium weight powder (Sigma-Aldrich, 448877) dissolved in acetic acid solution (1% v/v in deionized

water). The solution was stirred overnight at RT until complete dissolution. The obtained solution was filtered using a Büchner funnel with Perfecte2 filter paper with a 10 μm cut-off (Superfiltro Milano) and a vacuum pump, slowly bringing the system to low pressures (around 250–300 mbar). This solution was stocked at 4 °C for multiple preparations of Chi films.

Glycerol 10% in volume was added fresh to the Chi solution at each film preparation. The Gly-Chi solution was stirred for 30 min, until complete homogeneity. The Gly-Chi solution was sonicated for 15 min just before use and poured on the patterned area of the PDMS mold, placed in a 35 mm Petri dish. For each mold (total size around 8 cm^2), 0.5 g of glycerol-Chi solution was used. The molds covered with glycerol-Chi solution were kept for 72 h under chemical hood at RT, until the films had completely dried.

The films were neutralized for 30 min in a 0.5% w/v NaOH solution (0.5 g NaOH in 100 mL DI-water) and washed once with phosphate buffered solution (PBS; Sigma-Aldrich, D8537). Before cell culturing, Gly-Chi membranes were sterilized by treatment with ethanol 70% (for 15 min) and then rinsed with sterile H₂O Milli-Q. The membranes were then coated with a solution of Poly-L-Lysine (PLL 0.007% in water, at RT for 30 min; Sigma-Aldrich, P4832) for proper cell adhesion. For selected experiments, we also produced chitosan membranes (Chi), as previously [14].

4.3. Microtopography characterization by bright-field imaging

GR and SCA microstructured Gly-Chi films were analyzed to ensure the correct transfer of the pattern from the molds. The Gly-Chi films were imaged using a 20x air Nikon objective (N.A. 0.45, PlanFluor) with an Eclipse-*ti* inverted wide-field microscope (Nikon, Japan).

4.4. AFM

AFM was used to quantitatively analyze the Gly-Chi membrane patterns with a Bruker Dimension Icon microscope operating in ScanAsyst mode (Bruker, Billerica, MA, USA). Samples were measured at RT and pressure, under air atmosphere. Data were elaborated using Gwyddion software (Gwyddion version 2.63, Brno, Czech Republic, available at <http://gwyddion.net/>) and reported as the mean \pm standard deviation (SD) from sets of 4–10 measurements for each topography type.

4.5. Thermal analysis

TGA was performed on a Q500 instrument (TA Instruments, New Castle, DE, USA). Samples were analyzed under a nitrogen flow of 60 ml min^{-1} in the temperature range of 30 °C–700 °C, at a heating rate of 10 °C min^{-1} . Maximum temperatures (T_{max}) were taken as peaks in the first derivative of the TGA thermograms. DSC analysis was performed on

a DSC-822 instrument (Mettler-Toledo International Inc., Columbus, OH, USA). Samples were analyzed in the temperature range of 25 °C–200 °C, with a heating and cooling rate of 10 °C min⁻¹, under a nitrogen flow of 80 ml min⁻¹. Polymer glass transition temperature (T_g) was taken at the inflection point in the first and second heating thermograms.

4.6. Uniaxial tension tests

Mechanical tests were performed on an Instron 5564 uniaxial testing machine (Instron, Norwood, MA, USA) equipped with a 2 kN load cell. Samples were fixed to pneumatic tensile clamps by applying a grippy air pressure of 1.8 atm. An elongation rate of 1 mm min⁻¹ was applied. Stress was defined as the measured force divided by the initial cross-sectional area of the sample. Strain was defined as the ratio between length variation and initial length, and reported as %. In the stress–strain curves, the tensile modulus was calculated as the slope of the initial linear region, the tensile stress (σ_T) and strain at break (ε_T) were calculated at the breaking point. Six replicates were measured for the analysis and data were reported as mean \pm SD.

4.7. Membranes degradation test

The films were neutralized with the protocol described above, then dried with blotting paper. After that, they were weighted and submerged in a lysozyme solution (Thermo Scientific, 89833). We tested two different concentrations, 10 mg l⁻¹ and 100 mg l⁻¹. PBS was used as a control. The Gly-Chi films in solution were kept on a rocking table at 90 rpm at 37 °C. The membranes were weighted, after drying with blotting paper, after 3, 7, 14, 21 d and after 1, 2 and 3 months. The membranes were imaged with a 20x air Nikon objective (N.A. 0.45, PlanFluor) and Eclipse-Ti inverted wide-field microscope (Nikon, Japan) after 2 and 3 months.

4.8. SC line culture

For cell-material interaction experiments, the RT4-D6P2T cell line (ATCC CRL-2768), a Schwannoma cell line derived from a rat peripheral neuro-tumor and transduced with a lentivirus to stably express the GFP, was used [14, 46, 48]; these cells were kindly provided by Prof. Giovanna Gambarotta (Univ. of Turin, Italy).

RT4-D6P2T-GFP SCs (hereinafter referred to as RT4-SCs) were cultured and maintained at 37 °C in a humidified atmosphere of 5% CO₂/air, in Dulbecco's modified Eagle's medium supplemented with 4.5 g l⁻¹ glucose, 100 U ml⁻¹ penicillin, 100 µg ml⁻¹ streptomycin, 0.11 g l⁻¹ sodium pyruvate, 4 mM L-glutamine, and 10% heat-inactivated fetal bovine serum. All products were by Thermo-Fisher Scientific (Waltham, MA, USA).

4.9. Single cell migration experiments

RT4-SCs were seeded on FLAT, GR, and SCA Chi-glycerol films at a concentration of 10 000 cells cm⁻². After 24 h, living-cell imaging was performed using a 20x air Nikon objective (N.A. 0.45, PlanFluor) and Eclipse-Ti inverted wide-field microscope (Nikon, Japan) equipped with a perfect focus system, an incubating chamber (Okolab, Italy) and a CCD ORCA R2 (Hamamatsu, Japan). Bright-field and fluorescent images were acquired for 20 h, sampling every 10 min. Tracks were traced on GFP-fluorescence images and analyzed with the ImageJ manual tracking plugin MTrack, and by a custom-made Matlab script, as in Scaccini 2021. The following parameters were measured: (1)- *migration steps* (dS; corresponding to the cell motion calculated in 10 min): step vectors were analyzed along two directions, and dS was considered parallel (dS_{||}) if the angle between the step and the GR was between 0° and 15°, while it was considered perpendicular (dS_⊥) for angle between 75° and 90°. The amount of *parallel* or *perpendicular* dS was reported as percentage over the dS total number. (2)- *cell displacement* (the distance, in µm, from the origin after 15 h). (3)- *average cell speed* (V, in µm h⁻¹): as previously for dS, the average speed was also quantified as parallel (V_{||}); (4)- *persistence* (the percentage of parallel steps in the predominant direction of migration of the cells), such as an indicator of the probability of the cell to persist in one direction of migration instead of reverting it, along the main axis of the pattern. At least, 15 cells per condition were tracked for each substrate. We performed $n = 3$ independent experiment for each condition.

4.10. Wound healing experiments

Wound healing measurements were performed on monolayers of RT4-SCs, on Gly-Chi membranes. The cells were seeded on Chi films in two monolayers separated by a gap (average size $W_{\text{mean}} = 300 \pm 61$ µm, mean \pm SD) perpendicular to the pattern (or along a random direction in the case of FLAT membranes) thanks to PDMS culture-inserts with 2 wells (81176, IBIDI GMBH), at a concentration of 80 000 cells cm⁻². The day after, the PDMS culture-inserts were removed ($t = 0$) and images were acquired using a Nikon-Ti wide field microscope (see above) by using a 20x objective (Nikon). Wound healing time series were recorded by time-lapse microscopy and the wound area was measured in time until closure (around 9–10 h). The percentage of area closure after 5 h was finally reported. At least, $n = 3$ independent experiments were performed for each substrate type. As comparison, we also quantified the wound area after 10 h on Chi membranes, from [14].

4.11. Immunostaining and confocal imaging

RT4-SCs were grown for 3 d on FLAT, GR, and SCA Gly-Chi membranes, then fixed for 15 min

in 4% paraformaldehyde in PBS at RT and processed as previously reported [14]. Cells were stained with primary antibodies in GDB buffer (0.2% BSA, 0.8 M NaCl, 0.5% Triton X-100, 30 mM phosphate buffer, pH 7.4) containing phalloidin-Alexa647 (Invitrogen A22287; 1:40) to stain actin fibers (F-Actin), overnight at 4 °C. Primary antibodies: anti- β -Catenin (Non-phospho (Active) β -Catenin, Cell Signalling, 8814 S, 1:100, rabbit); anti-N-Cadherin (N-Cad; BD Transduction Lab, codice; 1:150, mouse); anti-YAP1 antibody (YAP, AbCam ab39361; 1:500). Samples were then washed and incubated with appropriate AlexaFluor Plus-488 or -594 conjugated secondary antibodies (ThermoFisher; 1:100) in GDB for 1 h at RT. After washing, samples were mounted using Fluoroshield histology mounting medium with 4',6-diamidino-2-phenylindole (DAPI) (Sigma-Aldrich, F6182).

The samples were imaged using a Zeiss LSM 800 (Jena, 439 Germany) inverted confocal microscope with a 40×1.5 numerical aperture oil immersion objective using 3 laser lines (405, 561, and 647 nm). The pinhole aperture was set at 1.0 airy. Each reported confocal image was obtained from a z-series (stack-depth was within 10 μm ; steps = 1 μm).

Each reported confocal image was obtained from a z-series (stack-depth was within 10 μm ; steps = 1 μm). The resulting z-stack was processed by ImageJ software (NIH, USA) into a single image using 'z-project' and 'Max intensity' options. The confocal settings were kept the same for all scans when fluorescence intensity was compared.

4.12. Cell morphological analysis

The confocal images of actin fibers were used to evaluate protrusions morphology by ImageJ (NIH), as in [14]. The orientation of the patterns was measured by the 'Angle tool' of ImageJ. Cell protrusions' contours were drawn by the 'Polygon selection' tool and analyzed by the 'Measurement' tool (with the options 'Area', and 'Mean gray value'). Being almost all cells bipolarized on micro-patterns, the parameters measured in this analysis were: the ratio of protrusions' area (the ratio between the area of the two cell's protrusions, the bigger one over the minor one), as parameter of *cell-ends asymmetry*; the ratio of actin signal intensity between the two cell protrusions (the ratio between the actin mean intensity of the bigger protrusion and the minor one, for each cell), as parameter of *cell-ends contractility asymmetry*. Each protrusion's area was drawn with a fixed length of 15 μm (i.e. along the cell & underlying pattern main axis, in some direction), with the aim to analyze the same segment in all cells and to avoid soma compartment. At least 12 cells were analyzed per sample.

RT4-SC *nucleus, cytoskeleton and cell-cell junctions' organization* were quantified as in [14]. We analyzed the actin fibers, β -Catenin and N-Cad

fluorescence signals with the 'Directionality' tool of the software FIJI (<http://fiji.sc/Fiji>). This plugin returned a directionality histogram by exploiting image FFT algorithms: isotropic images generate a flat histogram, whereas oriented images give a peaked histogram. These histograms were finally fitted by Gaussian curves that returned two parameters, *dispersion*, and *directionality* (the SD and the center of the Gaussian curve, respectively), the first representing the degree of orientation of the image, the second the direction in which it is oriented (here normalized to the underlying pattern orientation direction). We analyzed at least five fields/sample; image dimensions were kept fixed to $160 \times 160 \mu\text{m}^2$. For *nucleus analysis*, the nuclei perimeter was drawn with the 'Wand Selection' tool (that draws an ellipse around the nuclei) and processed with the 'Measurement' tool in ImageJ, and the nuclear aspect ratio and alignment angle were reported. We analyzed at least 30 nuclei/sample.

The YAP signal was quantified by ImageJ as in [45]. Briefly, the cell or nucleus were drawn as ROI on the respective F-Actin or DAPI images, and applied to the correspondent YAP images and here YAP intensity was measured by the ImageJ 'Measure' tool (option 'mean grey value') in nuclei and whole-cells minus nuclei. The values were then reported as the nuclear/cellular ratio; at least 20 cells/sample were analyzed. We performed $n \geq 3$ independent experiments for each condition.

4.13. RNA isolation, cDNA preparation and quantitative real-time PCR (qRT-PCR)

Total RNA was isolated using the QIAzol Lysis Reagent (79306, Qiagen) according to the manufacturer's instructions. RT4-SCs cultured on two GlyChi membranes were put together to form a sample for each RNA extraction (using 700 μl of QIAzol for each membrane). Total RNA was extracted using the miRNeasy Mini Kit (Qiagen, 217004), following manufacturer's instructions. cDNA was produced using the iScriptTM cDNA Synthesis Kit (Bio-Rad, 1708891), using 1 μg of total RNA as an input. The reaction was performed at 25 °C 5 min, at 46 °C 20 min, at 95 °C 1 min. Quantitative real-time PCR was performed using a 7300 Real-Time PCR System (Applied Biosystems, Life Technologies Europe BV, Italy). cDNA was diluted four folds in nuclease-free water and then 50 ng of initial RNA were analyzed in a 10 μl reaction volume, containing 5 μL SsoAdvancedTM Universal Inhibitor-Tolerant SYBR[®] Green Supermix (1725017, BioRad) with 10 μM forward and reverse primers.

Dissociation curves were routinely performed to check for the presence of a single peak corresponding to the required amplicon. Analysis was performed in technical and biological triplicate. The CT values were

then processed by the dCT method: for each candidate gene, the average dCT value are calculated for all the samples subtracting the average CT value from the CT value of the housekeeping gene. Then, the dCT value is calculated by subtracting the dCT value of the sample from the dCT value of the control condition (here standard plastic well). Finally, applying the equation $2(-ddCt)$ to all the samples, the expression of the analyzed genes is expressed in respect to the control condition, which is equal to 1. We investigated the expression of glial markers: S100 (forward primer 5'-3' GGGTGACAAGCACAAGCTGAAGAA, reverse primer 3'-5' TTGTCCACCACTTCCTGCTCTTTG), as in [46]; MBP (FW primer 5'-3' GGACCCAAGATGAAAACCCAGTAGTCC, RV primer 3'-5' CCTTTCCTGGGATGGAGGGGG); BDNF (FW primer 5'-3' GCGTGTGTGACAGTATTAGCGAGTG, RV primer 3'-5' CTCAGTTGGCCTTTTGATACCGG). Data were analyzed by $\Delta\Delta C_t$ relative quantification method normalizing to the housekeeping gene Tata-box Binding Protein (TBP) (FW primer 5'-TAAGGCTGGAAGGCCCTGTG-3'; RV primer 5'-TCCAGGAAATAATTCTGGCTCATAG-3').

4.14. Statistical analysis

All the experiments were repeated at least three times independently for each condition. Data are reported as the average value \pm the standard error of the mean (mean \pm SEM), unless differently stated. The mean values obtained in each repeated experiment were assumed to be normally distributed about the true mean. One-Way ANOVA (Bonferroni multiple comparison test) analysis was used, unless differently stated, to compare Gly-Chi substrates. Student's *t*-test (*unpaired*) was used to compare two conditions (here, Gly-Chi vs. Chi-100%). Statistical significance refers to results where $P < 0.05$ was obtained.

Data availability statement


All data that support the findings of this study are available in Zenodo repository at this link: [10.5281/zenodo.13683985](https://zenodo.org/record/13683985) [49].

Acknowledgments

This research was funded by the projects: PRIN 2022 - 2022ZH5M72 (PE11) - ENGINerve - "Development of nano/micro-engineered devices for applications in peripheral nervous system pathological models", financed by PNRR Missione 4 - Componente 2 - Investimento 1.1 "Fondo per il Programma Nazionale di Ricerca e Progetti di Rilevante Interesse Nazionale (PRIN)", European Union - Next Generation EU; PRIN 2020- ToaC- "Touch on a chip", financed by Italian Ministry of Research and University.

ORCID iDs

L Scaccini  <https://orcid.org/0000-0003-1844-1579>

I Tonazzini  <https://orcid.org/0000-0002-7323-2174>

References

- [1] Murphy R N A, de Schoulepnikoff C, Chen J H C, Columb M O, Bedford J, Wong J K and Reid A J 2023 The incidence and management of peripheral nerve injury in England (2005–2020) *J. Plast. Reconstr. Aesthet. Surg.* **80** 75–85
- [2] Whalley K 2016 Neural repair: networking for regeneration *Nat. Rev. Neurosci.* **17** 197
- [3] Jessen K R and Mirsky R 2019 The success and failure of the schwann cell response to nerve injury *Front. Cell Neurosci.* **13** 33
- [4] Huang D X, Yang M-X, Jiang Z-M, Chen M, Chang K, Zhan Y-X and Gong X 2023 Nerve trunk healing and neuroma formation after nerve transection injury *Front. Neurol.* **14** 1184246
- [5] Johnson E O and Soucacos P N 2008 Nerve repair: experimental and clinical evaluation of biodegradable artificial nerve guides *Injury* **39** S30–6
- [6] Schon B S, Hooper G J and Woodfield T B 2017 Modular tissue assembly strategies for biofabrication of engineered cartilage *Ann. Biomed. Eng.* **45** 100–14
- [7] Jiang X et al 2010 Current applications and future perspectives of artificial nerve conduits *Exp. Neurol.* **223** 86–101
- [8] Sarker M et al 2018 Strategic design and fabrication of nerve guidance conduits for peripheral nerve regeneration *Biotechnol. J.* **13** e1700635
- [9] Yan Y et al 2022 Implantable nerve guidance conduits: material combinations, multi-functional strategies and advanced engineering innovations *Bioact. Mater.* **11** 57–76
- [10] Tonazzini I and Cecchini M 2017 *Neuronal Mechanisms for Nanotopography Sensing Ebook Frontiers in Nanomedicine: Nanomedicine and Neurosciences: Advantages, Limitations and Safety Aspects* (Bentham Science Publishers) pp 101–14
- [11] Ferrari A, Cecchini M, Serresi M, Faraci P, Pisignano D and Beltram F 2010 Neuronal polarity selection by topography-induced focal adhesion control *Biomaterials* **31** 4682–94
- [12] Ferrari A, Cecchini M, Dhawan A, Micera S, Tonazzini I, Stabile R, Pisignano D and Beltram F 2011 Nanotopographic control of neuronal polarity *Nano Lett.* **11** 505–11
- [13] Tonazzini I, Meucci S, Faraci P, Beltram F and Cecchini M 2013 Neuronal differentiation on anisotropic substrates and the influence of nanotopographical noise on neurite contact guidance *Biomaterials* **34** 6027–36
- [14] Scaccini L, Mezzena R, De Masi A, Gagliardi M, Gambarotta G, Cecchini M and Tonazzini I 2021 Chitosan micro-grooved membranes with increased asymmetry for the improvement of the schwann cell response in nerve regeneration *Int. J. Mol. Sci.* **22** 7901
- [15] Tonazzini I, Jacchetti E, Meucci S, Beltram F and Cecchini M 2015 Schwann cell contact guidance versus boundary-interaction in functional wound healing along nano and microstructured membranes *Adv. Healthcare Mater.* **4** 1849–60
- [16] Tang Q Y, Qian W X, Xu Y H, Gopalakrishnan S, Wang J Q, Lam Y W and Pang S W 2015 Control of cell migration direction by inducing cell shape asymmetry with patterned topography *J. Biomed. Mater. Res. A* **103** 2383–93
- [17] Dash M, Chiellini F, Ottenbrite R M, Chiellini E et al 2011 Chitosan—A versatile semi-synthetic polymer in biomedical applications *Prog. Polym. Sci.* **36** 981–1014

- [18] Pavinatto A, de Almeida Mattos A V, Malpass A C G, Okura M H, Balogh D T and Sanfelice R C 2020 Coating with chitosan-based edible films for mechanical/biological protection of strawberries *Int. J. Biol. Macromol.* **151** 1004–11
- [19] Meng Q, Heuzey M-C and Carreau P J 2014 Hierarchical structure and physicochemical properties of plasticized chitosan *Biomacromolecules* **15** 1216–24
- [20] Ma X, Qiao C, Wang X, Yao J and Xu J 2019 Structural characterization and properties of polyols plasticized chitosan films *Int. J. Biol. Macromol.* **135** 240–5
- [21] Smith D R, Escobar A P, Andris M N, Boardman B M and Peters G M 2021 Understanding the molecular-level interactions of glucosamine-glycerol assemblies: a model system for chitosan plasticization *ACS Omega* **6** 25227–34
- [22] Kusmono M W W and Lubis F I 2021 Fabrication and Characterization of Chitosan/Cellulose Nanocrystal/Glycerol Bio-Composite Films *Polymers* **13** 1096
- [23] Rivero S, Damonte L, García M A and Pinotti A 2016 An insight into the role of glycerol in chitosan films *Food Biophys.* **11** 117–27
- [24] Caroni J G et al 2021 Chitosan-based glycerol-plasticized membranes: bactericidal and fibroblast cellular growth properties *Polym. Bull.* **78** 4297–312
- [25] Crosio A, Fornasari B, Gambarotta G, Geuna S, Raimondo S, Battiston B, Tos P and Ronchi G 2019 Chitosan tubes enriched with fresh skeletal muscle fibers for delayed repair of peripheral nerve defects *Neural Regen. Res.* **14** 1079–84
- [26] Shapira Y et al 2016 Comparison of results between chitosan hollow tube and autologous nerve graft in reconstruction of peripheral nerve defect: an experimental study *Microsurgery* **36** 664–71
- [27] Neubrech F, Sauerbier M, Moll W, Seegmüller J, Heider S, Harhaus L, Bickert B, Kneser U and Kremer T 2018 Enhancing the outcome of traumatic sensory nerve lesions of the hand by additional use of a chitosan nerve tube in primary nerve repair: a randomized controlled bicentric trial *Plast. Reconstr. Surg.* **142** 415–24
- [28] Fornasari B E, Xu F and Gao L 2020 Natural-based biomaterials for peripheral nerve injury repair *Front. Bioeng. Biotechnol.* **8** 8
- [29] Barriga E H, Franze K, Charras G and Mayor R 2018 Tissue stiffening coordinates morphogenesis by triggering collective cell migration *in vivo Nature* **554** 523–7
- [30] Koser D E et al 2016 Mechanosensing is critical for axon growth in the developing brain *Nat. Neurosci.* **19** 1592–8
- [31] Romero L O, Massey A E, Mata-Daboin A D, Sierra-Valdez F J, Chauhan S C, Cordero-Morales J F and Vásquez V 2019 Dietary fatty acids fine-tune Piezo1 mechanical response *Nat. Commun.* **10** 1200
- [32] Evans E B, Brady S W, Tripathi A and Hoffman-Kim D 2018 Schwann cell durotaxis can be guided by physiologically relevant stiffness gradients *Biomater. Res.* **22** 14
- [33] Zhang M, Wang Y, Geng J, Zhou S and Xiao B 2019 Mechanically activated piezo channels mediate touch and suppress acute mechanical pain response in mice *Cell Rep.* **26** 1419–31.e4
- [34] Rosso G and Guck J 2019 Mechanical changes of peripheral nerve tissue microenvironment and their structural basis during development *APL Bioeng.* **3** 036107
- [35] De Masi A, Tonazzini I, Masciullo C, Mezzena R, Chiellini F, Puppi D and Cecchini M 2019 Chitosan films for regenerative medicine: fabrication methods and mechanical characterization of nanostructured chitosan films *Biophys. Rev.* **11** 807–15
- [36] Souza V G L et al 2019 Physical and morphological characterization of chitosan/montmorillonite films incorporated with ginger essential oil *Coatings* **9** 700
- [37] Kumar S and Koh J 2012 Physicochemical, optical and biological activity of chitosan-chromone derivative for biomedical applications *Int. J. Mol. Sci.* **13** 6102–16
- [38] Yadav S and Suroolia A 2019 Lysozyme elicits pain during nerve injury by neuronal Toll-like receptor 4 activation and has therapeutic potential in neuropathic pain *Sci. Transl. Med.* **11** eaav4176
- [39] Nectow A R, Marra K G and Kaplan D L 2012 Biomaterials for the development of peripheral nerve guidance conduits *Tissue Eng. B* **18** 40–50
- [40] Gu Y et al 2012 The influence of substrate stiffness on the behavior and functions of Schwann cells in culture *Biomaterials* **33** 6672–81
- [41] Wang T et al 2017 Extracellular matrix stiffness and cell contractility control RNA localization to promote cell migration *Nat. Commun.* **8** 896
- [42] Doss B L et al 2020 Cell response to substrate rigidity is regulated by active and passive cytoskeletal stress *Proc. Natl Acad. Sci. USA* **117** 12817–25
- [43] Tricaud N et al 2005 Adherens junctions in myelinating Schwann cells stabilize Schmidt-Lanterman incisures via recruitment of p120 catenin to E-cadherin *J. Neurosci.* **25** 3259–69
- [44] Blaschuk O W 2022 Potential therapeutic applications of N-cadherin antagonists and agonists *Front. Cell Dev. Biol.* **10** 866200
- [45] Tonazzini I et al 2020 Neuronal contact guidance and YAP signaling on ultra-small nanogratings *Sci. Rep.* **10** 3742
- [46] Pascal D et al 2014 Characterization of glial cell models and in vitro manipulation of the neuregulin1/ErbB system *BioMed. Res. Int.* **2014** 310215
- [47] Yi S et al 2016 Regulation of Schwann cell proliferation and migration by miR-1 targeting brain-derived neurotrophic factor after peripheral nerve injury *Sci. Rep.* **6** 29121
- [48] Gnani S et al 2017 Gelatin-based hydrogel for vascular endothelial growth factor release in peripheral nerve tissue engineering *J. Tissue Eng. Regen. Med.* **11** 459–70
- [49] Scaccini L et al 2024 Data set *Zenodo* <https://doi.org/10.5281/zenodo.13683985>